

# Document made available under the Patent Cooperation Treaty (PCT)

International application number: PCT/IB2005/001252

International filing date: 08 April 2005 (08.04.2005)

Document type: Certified copy of priority document

Document details: Country/Office: US  
Number: 60/560,898  
Filing date: 08 April 2004 (08.04.2004)

Date of receipt at the International Bureau: 06 June 2005 (06.06.2005)

Remark: Priority document submitted or transmitted to the International Bureau in compliance with Rule 17.1(a) or (b)



World Intellectual Property Organization (WIPO) - Geneva, Switzerland  
Organisation Mondiale de la Propriété Intellectuelle (OMPI) - Genève, Suisse

1325709

# THE UNITED STATES OF AMERICA

TO ALL TO WHOM THESE PRESENTS SHALL COME:

UNITED STATES DEPARTMENT OF COMMERCE

United States Patent and Trademark Office

May 24, 2005

THIS IS TO CERTIFY THAT ANNEXED HERETO IS A TRUE COPY FROM THE RECORDS OF THE UNITED STATES PATENT AND TRADEMARK OFFICE OF THOSE PAPERS OF THE BELOW IDENTIFIED PATENT APPLICATION THAT MET THE REQUIREMENTS TO BE GRANTED A FILING DATE.

APPLICATION NUMBER: 60/560,898

FILING DATE: April 08, 2004

RELATED PCT APPLICATION NUMBER: PCT/US05/12199



Certified by

Under Secretary of Commerce  
for Intellectual Property  
and Director of the United States  
Patent and Trademark Office

040804

17364 U.S. PTO

PTO/SB/16 (01-04)

Approved for use through 07/31/2006. OMB 0651-0032

U.S. Patent and Trademark Office; U.S. DEPARTMENT OF COMMERCE

Under the Paperwork Reduction Act of 1995, no persons are required to respond to a collection of information unless it displays a valid OMB control number.

**PROVISIONAL APPLICATION FOR PATENT COVER SHEET**

This is a request for filing a PROVISIONAL APPLICATION FOR PATENT under 37 CFR 1.53(c).

Express Mail Label No. EV 333610776 US

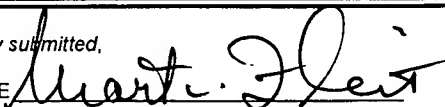
17513 U.S. PTO  
60/560898

INVENTOR(S)					
Given Name (first and middle [if any])		Family Name or Surname		Residence (City and either State or Foreign Country)	
Hadassah Daphna		DEGANI WEINSTEIN		Rehovot, ISRAEL Rehovot, ISRAEL	
Additional inventors are being named on the _____ separately numbered sheets attached hereto					
<b>TITLE OF THE INVENTION (500 characters max)</b>					
APPLICATION OF THE 3TP METHOD FOR LUNG CANCER DIAGNOSIS BY CT					
Direct all correspondence to: <b>CORRESPONDENCE ADDRESS</b>					
<input checked="" type="checkbox"/> Customer Number: <span style="border: 1px solid black; padding: 5px; display: inline-block; width: 200px; text-align: center;">27317</span>					
OR					
<input checked="" type="checkbox"/> Firm or Individual Name: MARTIN FLEIT					
Address: FLEIT KAIN GIBBONS GUTMAN BONGINI & BIANCO					
Address: 601 BRICKELL KEY DRIVE - SUITE 404					
City: MIAMI		State: FLORIDA		Zip: 33131	
Country: USA		Telephone: 3054164490		Fax: 3054164489	
<b>ENCLOSED APPLICATION PARTS (check all that apply)</b>					
<input checked="" type="checkbox"/> Specification Number of Pages <u>32</u>					
<input checked="" type="checkbox"/> Drawing(s) Number of Sheets <u>INCLUDED</u>					
<input type="checkbox"/> Application Data Sheet. See 37 CFR 1.76					
<input type="checkbox"/> CD(s), Number _____					
<input type="checkbox"/> Other (specify) _____					
METHOD OF PAYMENT OF FILING FEES FOR THIS PROVISIONAL APPLICATION FOR PATENT					
<input checked="" type="checkbox"/> Applicant claims small entity status. See 37 CFR 1.27.					
<input type="checkbox"/> A check or money order is enclosed to cover the filing fees.					
<input checked="" type="checkbox"/> The Director is hereby authorized to charge filing fees or credit any overpayment to Deposit Account Number: <u>500601</u>					
<input type="checkbox"/> Payment by credit card. Form PTO-2038 is attached.					
<div style="border: 1px solid black; padding: 5px; display: inline-block;">           FILING FEE Amount (\$)           <div style="border: 1px solid black; padding: 5px; display: inline-block; margin-top: 10px;">\$80.00</div> </div>					
The invention was made by an agency of the United States Government or under a contract with an agency of the United States Government.					
<input checked="" type="checkbox"/> No.					
<input type="checkbox"/> Yes, the name of the U.S. Government agency and the Government contract number are: _____					

[Page 1 of 2]

Respectfully submitted,

SIGNATURE



TYPED or PRINTED NAME MARTIN FLEIT

TELEPHONE 305-416-4490

Date APRIL 8, 2004

REGISTRATION NO. 16,900

(if appropriate)

Docket Number: 7040-X04-067P

**USE ONLY FOR FILING A PROVISIONAL APPLICATION FOR PATENT**

This collection of information is required by 37 CFR 1.51. The information is required to obtain or retain a benefit by the public which is to file (and by the USPTO to process) an application. Confidentiality is governed by 35 U.S.C. 122 and 37 CFR 1.14. This collection is estimated to take 8 hours to complete, including gathering, preparing, and submitting the completed application form to the USPTO. Time will vary depending upon the individual case. Any comments on the amount of time you require to complete this form and/or suggestions for reducing this burden, should be sent to the Chief Information Officer, U.S. Patent and Trademark Office, U.S. Department of Commerce, P.O. Box 1450, Alexandria, VA 22313-1450. DO NOT SEND FEES OR COMPLETED FORMS TO THIS ADDRESS. SEND TO: Mail Stop Provisional Application, Commissioner for Patents, P.O. Box 1450, Alexandria, VA 22313-1450.

If you need assistance in completing the form, call 1-800-PTO-9199 and select option 2.

# **A NOVEL CT METHOD FOR LUNG CANCER DETECTION AND DIAGNOSIS**

**Dr. Daphna Weinstein  
Asaf Harofeh Hospital**

Supervision: Prof. Hadassa Degani  
Weizmann Institute of Science

## **Abstract :**

Lung cancer forms the leading cause of death among cancers. Therefore, early detection is of utmost importance. Interestingly, the variety of routinely performed diagnostic tools has not yet led to a significant decline of the death rate. Thus, a non-invasive diagnostic technique would be desirable, as is the goal of this study. In our proposed method, contrast-enhanced dynamic information extracted from Computed Tomography( CT) images is obtained to characterize two independent pathophysiological parameters:  $K$  - the product of permeability and vascular surface area per voxel, and  $v$  - the fraction of extracellular space. A specific color coding scheme relates enhancement patterns to  $K$  and  $v$ . Their values and spatial distribution, as well as the morphological features extracted from the CT image, may enable to improve the differentiation between benign and malignant lung lesions. The principles of the method have already been developed and applied to MRI of breast and prostate cancer. In this study, the principles were further extended and a new algorithm was developed and applied to CT after adaptation to the lung physiology. The new method was tested on 30 suspicious pulmonary lesions, with result verification by histopathological findings.

# **Table of Contents**

## **I) SCIENTIFIC BACKGROUND 4 - 7**

- Risk factors for lung cancer
- Histological types
- Lung cancer presentation
- Radiological evaluation
- Treatment
- Prognosis
- The Solitary Pulmonary Nodule (SPN)
- Screening

## **II) SPECIFIC AIMS AND WORKING HYPOTHESIS 8**

## **III) MATERIALS AND METHODS 9 - 13**

- Patient Recruitment
- Imaging protocol and transfer
- Kinetic model of the contrast agent
- Image analysis by the 3TP algorithm
- Image interpretation and statistical evaluation

## **IV) RESULTS 14 - 23**

- Pharmacokinetics of Iopromide - Ultravist 300
- Image analysis

## **V) DISCUSSION 24 - 26**

## **VI) BIBLIOGRAPHY 27 - 29**

## **I) SCIENTIFIC BACKGROUND**

Lung cancer represents one of the major public health problems worldwide. It has been estimated that between 1.3 and 2 million people died from lung cancer during 2000. The number of deaths caused by lung cancer exceeds those caused by the next three leading cancers together per year (breast, prostate and colorectal) [1-3]. There is no doubt that decreasing mortality from lung cancer by improved diagnostic means will have an enormous influence on public health as well as reducing health care costs.

### **Risk factors for lung cancer**

Clearly, the major known risk factor is tobacco use, which is related to 80-85% of the cases. Up to 50% of lung cancers occur in former smokers, with the risk declining to that of non-smokers only after a few decades of smoking cessation [4]. Other risk factors include positive family history, advanced age, intrinsic factors, industrial materials, organic chemicals, radiation, air pollution, and exposure of non-smokers to smoke [2].

### **Histological types**

99% of the lung tumors are malignant, either primary or secondary.

**NSCLC** - Non-Small Cell Lung Carcinoma represents 80% of the bronchogenic carcinomas. Includes Adenocarcinoma, SCC (Squamous Cell Carcinoma), LCC (Large Cell Carcinoma), and more.

**SCLC** - Small Cell Lung Cancer - Oat Cell Carcinoma - forms the rest of the cases. It is the most aggressive type with a median survival of 2-4 months.

Less common types include Sarcoma, Carcinosarcoma, Blastoma, Lymphoma, Neuroendocrine tumors such as Carcinoids (both malignant and benign), and more [1-2,5-6].

### **Lung cancer presentation**

Half of the patients seek medical consultation when the disease has already advanced beyond surgical treatment. Since the lung parenchyma lacks nerve endings, tumors of the lung can become large before causing local symptoms such as cough (75%), dyspnea (60%), pain (50%) & hemoptysis (30%). Fever, wheezing, stridor, hoarseness, SVC (Superior Vena Cava) syndrome, Horner syndrome, dysphagia, pleural effusion, and phrenic nerve paralysis may occur as well. 70% of the patients have non-specific symptoms (anorexia, myalgia & weight loss), and the minority are asymptomatic. Some present with pneumonia due to bronchial obstruction, and some are diagnosed incidentally by a CXR (Chest X-Ray) assigned for another purpose [1].

## **Radiological evaluation**

Since pulmonary lesions are commonly encountered in clinical practice, differentiation of benign from malignant findings remains a challenge for the radiologist. A broad variety of diagnostic techniques is available, with others being developed.

i) **CXR** - Conventional Chest X-Ray is the basic diagnostic tool. It provides information regarding the size, shape, density and site of the lesion, apart for the existence of pleural effusions, alveolar or interstitial spread, collapse, lymphadenopathy, and rib metastases. An opacity is suspicious for malignancy if it isn't calcified, has spiculations, grows rapidly, or is >3 cm in diameter [7]. There are also hints about the histological type with Adenocarcinoma being peripheral, SCC central & large, and SCLC large, hilar, and with mediastinal lymphadenopathy. A lesion that hasn't grown in 2 years is considered benign [5].

ii) **CT** - Computed Tomography is the preferred modality for lung cancer diagnosis & staging. Contrast material helps differentiate between blood vessels and lymph nodes [7]. CT offers better evaluation of the tumor's borders, relation to neighboring structures, involvement of lymph nodes, bones, liver and adrenals [5]. Technical modifications of CT include: Low-dose helical CT (spiral CT), HRCT - High Resolution CT and Phase-contrast CT. Spiral CT provides higher spatial resolution than a CXR, at the expense of greater radiation exposure (in conventional CT the radiation exposure is greater by 10-100 than in a CXR, whereby spiral CT exposes to only 10-20% the exposure of conventional CT). It allows scanning of the whole lung during a single breath-hold of 8-25 seconds [8]. In functional CT, enhancement obtained by the contrast material is usually greater in malignant tumors due to their rich vascularity. Non-enhancement means no malignancy, although some benign tissues do enhance.

iii) **MRI** - Magnetic Resonance Imaging differentiates between solid and vascular structures, even without contrast material. Most importantly, MRI uses harmless radio waves and there is no exposure to ionizing radiation as in CT. The sensitivity and specificity of MRI are similar to those of CT. Due to longer acquisition time, patient movement is more detrimental [5,7,9].

iv) **Other methods** - Positron Emission Tomography (PET) using 18-fluorodeoxyglucose depicts increased glucose metabolism in tumor cells. This serves to evaluate the primary tumor as well as regional lymph nodes and distant metastases [5,10].

Percutaneous needle biopsy, flexible fiberoptic bronchoscopy as well as surgical exploration represent additional diagnostic tools. However, they are characterized by inherent invasiveness. Recent developments include exhalation analysis of certain volatile organic compounds, cytological sputum analysis, immunostaining for hnRNP, A2/B1 or PGP9.5, and polymerase chain reaction-based assays for detecting tumor-specific mutations [7,11-13].

## **Treatment**

Despite the various diagnostic modalities, 10-20% of the patients undergo thoracotomy without prior pathologic diagnosis. The exact treatment regimen depends on precise histological data before treatment and after excision. For stages I and II the preferred treatment is lobectomy followed by mediastinal lymphadenectomy for pathological staging. For stage IIIA pre-operative radiotherapy is recommended. More advanced stages are treated by chemotherapy or radiotherapy, with surgery offered only for palliation when needed [1,2].

## **Prognosis:**

Early detection leads to better prognosis. For example, in stage I the survival is 60-70% and in stage Ia even higher. Sadly, only 15% of the cases are diagnosed at an early stage (I and II) when the tumor is well localized, so the overall survival has not risen lately [11]. The 1-year survival has changed from 32% in 1973 to 41% in 1994. But, the overall 5-year survival is only 14% [1,2]. Concerning lung metastases, the prognosis depends on the type of primary tumor and its biological behavior. For some carcinomas and sarcomas, the 5-year survival after lung metastases excision is 25-45%.

## **The Solitary Pulmonary Nodule (SPN):**

The best survival is expected when lung cancer presents incidentally on a CXR as a “coin lesion”, or SPN, which is single, peripheral and asymptomatic. The SPN is defined as an abnormal round/oval density of diameter  $\leq 3$  cm, surrounded by lung parenchyma and lacking cavitations or pulmonary infiltrates. There could be eccentric flecks of calcifications, but not broad or concentric ring calcifications [2]. Approximately 80% of the coin lesions are malignant in patients of age  $>50$  years. Only when the lesion has been known to exist at least two years without enlarging and with a “benign” calcification pattern, could histological diagnosis be delayed. CT detects lesions  $>2$  mm, of which 45% are neoplastic. CT is superior to CXR by providing staging, volumetric, and density data (higher enhancement & size being more characteristic of malignancy) [14], and evaluation of the best method to obtain a biopsy, including needle localization for biopsy under VATS (Video Assisted Thoracoscopic Surgery) [15]. Advancement in SPN evaluation by CT has been made by improvements in image processing and computer assistance, named CAD (Computer-Aided Diagnosis) [16].

Only 50% of the lesions suspicious enough to undergo an open biopsy turn out to be malignant. This brings about not only needless morbidity and mortality, but the hospitalization costs of such a patient in the US are about 25,000\$. When a SPN is detected, it will represent primary



lung cancer in most breast cancer patients, and a metastasis in most melanoma patients. For cancer of the gastrointestinal tract the odds for both options are equal.

Follow-up of a SPN is usually dependent upon the lesion's diameter:

1. <5 mm: HRCT after 3,6,12 & 24 months. Consider biopsy if enlarges. 1% malignancy.
2. 5-10 mm: as above, but 25-30% malignancy.
3. >10 mm: consider biopsy. 30-80% malignancy.

It is important to note that there isn't a fixed relationship between the size of the nodule and its biological behavior. It is possible that most patients already have metastases at the time of diagnosis, which the routine diagnostic tools do not always detect. This hypothesis is supported by clinical studies in which lymph nodes that appeared normal were found to contain metastases when evaluated by immunohistochemical staining or PCR [5].

### **Screening:**

There is general agreement among the various health organizations in the US, that the screening programs customary until recently (CXR & sputum cytology), have not contributed significantly to decrease the death rate. This is not true for the next three most common cancers: breast, prostate and colorectal, for which the death rate has decreased by 10-15% in the past 2 decades. It should also be noted, that in the Johns Hopkins Lung Project from the 70's, screening tests were negative in half of the patients that developed lung cancer, and became symptomatic before the next scheduled screening examination. A possible explanation was that some of the cases are so aggressive, that even strict follow-up and early detection will not increase survival. Actually, screening is intended mainly for NSCLC (75-80% of the cases), since SCLC is usually widely disseminated at presentation [17].

Apart for attempts to improve existing detection modalities, the future challenge is to develop new techniques for the early detection of lung cancer. They might rely on studies in the fields of carcinogenesis, molecular biology and genetics [5].

## II) SPECIFIC AIMS AND WORKING HYPOTHESIS

We propose a novel CT method for the distinction between benign and malignant lung lesions. From previous results of the proposed method on MRI images of breast and prostate cancer, some common characteristics were found. For example, a malignant tumor was represented by a higher percentage of red pixels, which correlate to an area of high  $K$  & low  $v$ . The kind of tumor was also suspected from the amount of dispersement between the different colors. A uniform pattern of low cell-density characterized a benign process, while non-uniform scattering represented malignancy.

As the method is not specific for contrast-enhanced MRI or to a certain body area, we wanted to evaluate whether it is applicable to contrast-enhanced CT of suspicious pulmonary lesions.

Reasons leading us to choose the lungs include:

1. These Patients undergo a CT scan routinely, usually followed by a biopsy.
2. Lung cancer forms the leading cause of cancer death in the Western world today.  
Therefore, early diagnosis is of utmost importance both economically and health-wise.
3. Follow-up of suspicious lung lesions leads to undesired psychological stress.
4. To decrease the unnecessary morbidity and mortality caused by biopsies performed when there isn't convincing evidence that a lesion is benign (~50% of the cases).

The disadvantage of choosing the lungs is the issue of registration (shift/movement) that is detrimental in our case since we follow each pixel's enhancement as a function of time. Therefore we must also address the methods of correction we used in both x-y and z directions. In order to transform the 3TP-MRI algorithm to lung CT, we have done the following:

1. Defined the equations that characterize the dynamical enhancement by the contrast material.
2. Verified the relationship between the concentration of contrast material and signal intensity.
3. Evaluated the pharmacokinetics of the contrast agent.
4. Incorporated the above information into the 3TP algorithm.
5. Developed software to read CT images and calibrate their intensity at pixel resolution.
6. Selected the optimal acquisition times for the specific dose of contrast material and CT protocol, and verified the choice by theoretical iterations and experimentally.
7. Dealt with the tumor's motion between the different acquisitions, mainly due to breathing.
8. Tested the feasibility of the method to differentiate between benign and malignant disease in a cohort of 30 pulmonary lesions, with verification by histopathology.

### **III) MATERIALS AND METHODS**

#### **Patient Recruitment:**

We recruited 34 patients (22 men and 12 women; mean age 64 years; age range 47-82 years) referred to the radiology department either from the Thoracic Surgery Ward, or from the Pulmonary Outpatient Clinic to undergo a CT scan as part of their further clinical evaluation of a lung lesion, prior to performing a biopsy. The biopsy could be obtained by thoracotomy, thoracoscopy, mediastinoscopy, bronchoscopy or transcutaneic. Exclusion criteria included abnormal kidney function tests, a known allergy to iodine, age < 18 years, pregnancy and patients legally incapable of signing an informed consent. Informed consent was obtained according to the approval of the hospital's ethics committee.

#### **Imaging protocol and transfer:**

All images were obtained using the Mx8000 (Philips) Multi Detector CT (MDCT) scanner in the Department of Radiology in Asaf-Harofeh Medical Center. Acquisition of the CT images was performed by an experienced technician under the surveillance of an expert radiologist. First, a survey scan of the chest was performed. This scan served to plan the study so it will focus on the lung lesion. Consecutive scans of the lung lesion were then performed, with identical parameters. The first, prior to IV (Intra-Venous) contrast injection, and the next two at pre-determined time-points after IV contrast administration. A third scan was made for pharmacokinetic information only. The scan was performed with a 1.3 mm collimation (slice width) with a 1 mm slice interval, pitch 0.7, rot. time 0.75 sec, 120 kV tube voltage, 250 mAS. Voxel volume (pixel area x slice width) ranged between  $0.78 \times 0.78 \times 1.3 \text{ mm}^3$  (the majority) to  $0.98 \times 0.98 \times 1.3 \text{ mm}^3$ .

Since this is a pilot study, the optimal 2 post-contrast time points were not known apriori. Therefore, until enough data was collected for initial pharmacokinetic results, different time points were selected for each patient, all  $\leq 0$  minutes. This provided useful data for the pharmacokinetic evaluation as well. As the study progressed, the range of valuable time points became clearer.

The non-ionic contrast material Iopromide (Ultravist 300; Schering), at a dose of 1.5 ml/kg, was delivered through the antecubital vein at a rate of 3 ml/sec via an automatic injector (EnVision CT<sup>TM</sup> injector). During each scan the patients were instructed to hold their breath following maximal expiration in order to decrease registration problems. A scan specific to the tumor area takes a few seconds since total thoracic scanning lengths about 20 sec.

We chose the contrast agent Iopromide (1 ml containing 0.623 g Iopromide), since it is a non-ionic water-soluble X-ray contrast medium with low osmotic pressure and better general tolerance compared to ionic contrast media. It has a molecular weight of 791.12 d (compared to 936 d of GdDTPA/dimeglumine). It is extremely hydrophilic and prevented from entering the intracellular lumen [18-19]. Therefore, like Gd-DTPA, following IV administration iopromide is very rapidly distributed in the extracellular space, the half-life being 3 minutes, with an elimination half-life in patients of normal kidney function approximating 2 hours, irrespective of the dose (only 1.5% of the dosage is excreted in feces).

#### **Kinetic model of the contrast agent :**

The 3TP-CT method, which we have developed, is a modification of the method applied to GdDTPA-enhanced MRI, which was described in prior publications [20-23]. Our main purpose is to characterize histopathological properties of lung tumors by distinguishing between different time profiles of enhancement, which are related to the change in the contrast agent's concentration at 3 different time points. A multi-compartment exchange model describes the pharmacokinetics of the contrast material. According to this model, the body is divided into 4 compartments: intravascular, whole-body extracellular space, tumor extracellular space, and kidneys. The concentration of the contrast agent in the plasma as a function of time  $C_p(t)$  (in units of ml/lit), is represented by a bi-exponential equation [24]:

$$(1) \quad C_p(t) = D(a_1 e^{-m_1 t} + a_2 e^{-m_2 t})$$

where  $D$  is the dose of the contrast material (in units of ml/kg),  $m_1$  and  $m_2$  are the decay rates (in  $\text{min}^{-1}$ ) and  $a_1$  and  $a_2$  are the amplitudes (in kg/lit).

It is assumed, that after the end of bolus injection the concentration of the contrast agent in the plasma is uniform throughout the whole body, regardless of the injection site.

The term  $a_1 e^{-m_1 t}$  correlates with a phase of rapid distribution between the intravascular and extracellular compartments, and the term  $a_2 e^{-m_2 t}$  correlates with slower elimination of the contrast material by the kidneys.

The exchange of contrast material between the intravascular and extravascular space is dependent upon two parameters:  $v$  – the extracellular volume fraction accessible to the contrast agent, which is incapable of entering into cells, and  $K \sim PS/V$  (where  $P$  = microvascular permeability,  $S$  = microvascular surface area and  $V$  = pixel volume).

In the tissue, the concentration of the contrast agent is written as:

$$(2) \quad C_i(t) = D(b_1 e^{-m_1 t} + b_2 e^{-m_2 t} + b_3 e^{-m_3 t})$$

where  $b_1 = K a_1 / (K/v - m_1)$ ,  $b_2 = K a_2 / (K/v - m_2)$ ,  $b_3 = - (b_1 + b_2)$  and  $m_3 = K/v$ .

This equation represents an initial increase of  $C_i(t)$  with time, as the contrast material exits the blood vessels into the tumor's extracellular space, followed by a decrease as the contrast agent is cleared from the tumor back to the blood.

Note, that eq. (2) approaches eq. (1) when  $K \rightarrow \infty$  and  $v = 1$  as occurs in blood (fig. 1).

These equations are the same as those used for MRI, but the values of  $a_1$ ,  $a_2$ ,  $m_1$ , and  $m_2$  differ according to the contrast agent used.

### **Image analysis by the 3TP algorithm:**

For each pixel in the CT image, the relation between its measured signal intensity  $S(t)$  in HU (Hounsfield Units) and the concentration  $C(t)$  of contrast material within the voxel it represents ) is described by:

$$(3) \quad S(t) = p + qC(t)$$

where  $p$  and  $q$  are parameters to be determined.

We define enhancement,  $E(t)$ , as the difference in signal intensities before and after contrast material injection:

$$(4) \quad E(t) = S(t) - S(t_0)$$

Note that, by definition,  $E(t)$  must be positive.

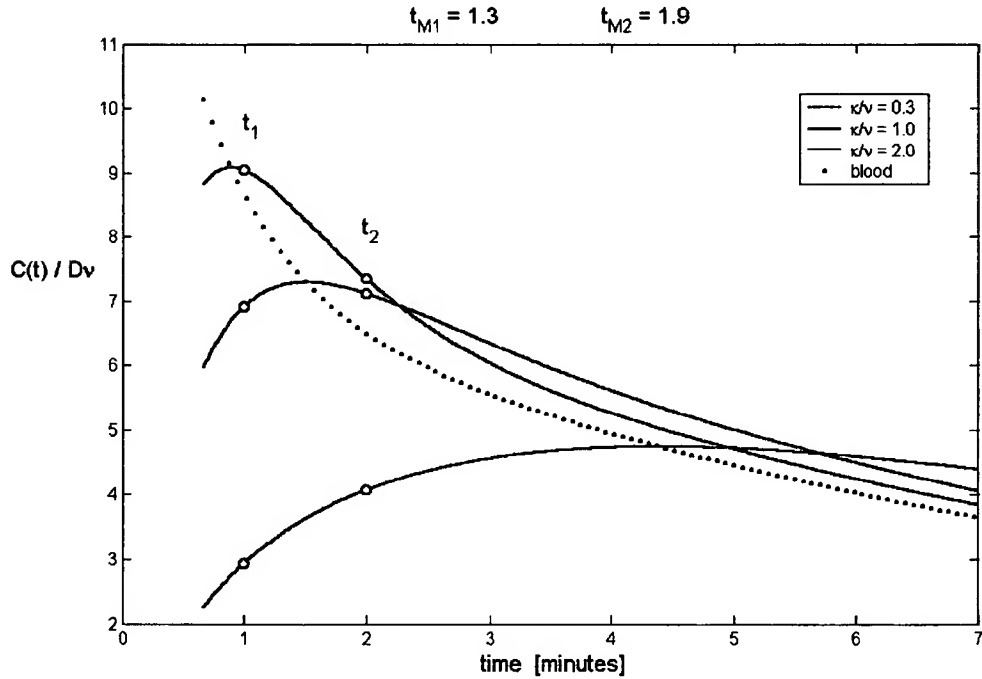
The objective of the 3TP-CT method is to evaluate the local values of  $K$  and  $v$  by analyzing CT images acquired at 3 different time points. The first scan is performed prior to IV contrast material injection, at time point  $t_0$ , and serves as a baseline. The following scans are performed  $t_1$  and  $t_2$  minutes after injection. The enhancements  $E(t_1)$  and  $E(t_2)$  of each pixel are translated using equations (3) and (4) into two equations of concentrations:  $C_i(t_1)$  and  $C_i(t_2)$ . These equations are solved numerically for the local values of  $K$  and  $v$ .

In order to give visual meaning to the solution of  $C_i(t)$  we distinguish between three time profiles, as presented in **fig. 1**.

For high  $K$  and low  $v$  the concentration reaches its maximal value shortly after the end of injection and then decays relatively fast. In the opposite case, of low  $K$  and high  $v$ , the increase of  $C(t)$  is much slower and its maximum is reached after a long time. Intermediate values of  $K$  and  $v$  will result in a point of maximal concentration in between the above ones.

To each pixel we assign a color hue according to the profile pattern its enhancement fits best. We color in red pixels with rapid enhancement whose maximal intensity is reached before a time we define as  $t_{m_1}$ , in blue those who reach a maximum later than a time we define as  $t_{m_2}$ , and in green the pixels whose maximal intensity is obtained between  $t_{m_1}$  and  $t_{m_2}$ .

**Fig. 1:** The three different concentration profiles according to the color-code.

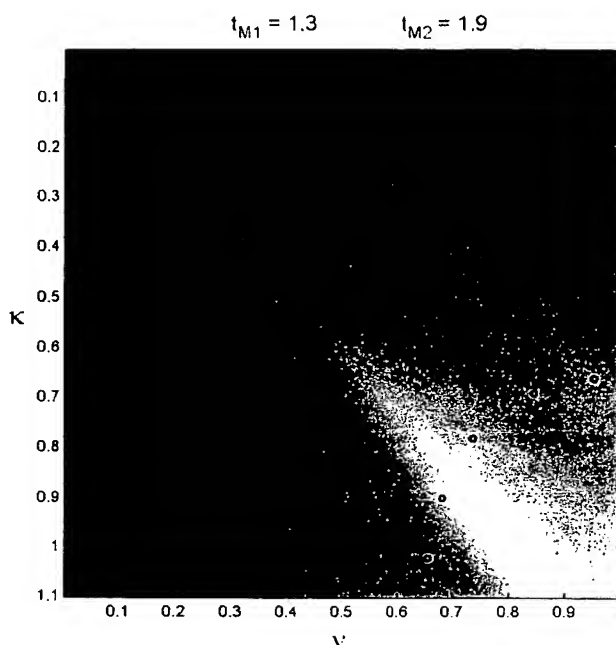


Note, that with the increase in  $K/v$  we approach the behavior of blood.

Also, it can be seen that in the red profile the concentration decreases between the scan times  $t_1$  and  $t_2$ , in the green profile it hardly changes, and in the blue one it increases.

In addition to color hue, each pixel is assigned a color brightness (ranging between 0 to 1) according to the enhancement  $E(t_1)$  at  $t_1$ . In this way, for a given  $t_{m_1}$  and  $t_{m_2}$ , we create a color map which assigns a color (hue and brightness) to every pair of  $K$  &  $v$  and thus enables the viewer of the color-coded CT-image to understand the histopathological characteristics of its different pixels [23-25].

Fig. 2: Color-map.



In **fig. 2** we present a color-map of the  $K$ - $v$  plane, which helps understand which  $K/v$  is represented by the color of each pixel. We choose  $t_{m_1}$  and  $t_{m_2}$  in such a way that will enable good resolution within the  $K$ - $v$  plane. This serves to extract maximal information regarding areas of different histological characteristics within the color-coded image.

The brightness increases from zero at the left upper corner towards one at the right lower corner. The circled curve depicts the maximal value of brightness equaling one. Lines of iso-brightness are of the same shape as the circled line within the map.

#### **Image interpretation and statistical evaluation:**

The localization of a lesion is made by observing enhancement in the original images, and by the 3TP method, which colors the regions that are enhanced and then relates them to  $K$  &  $v$ .

Analysis and statistical evaluation was done with special attention to the extent of pixels colored, the extent of pixels exhibiting each color hue; the brightness range, and the spatial distribution of the different colors (hue & brightness).

**A NOVEL CT METHOD FOR LUNG CANCER DETECTION AND  
DIAGNOSIS**

**Dr. Daphna Weinstein  
Asaf Harofeh Hospital**

Supervision: Prof. Hadassa Degani  
Weizmann Institute of Science

Part B



## IV) RESULTS

### a) Pharmacokinetics of Iopromide - Ultravist 300

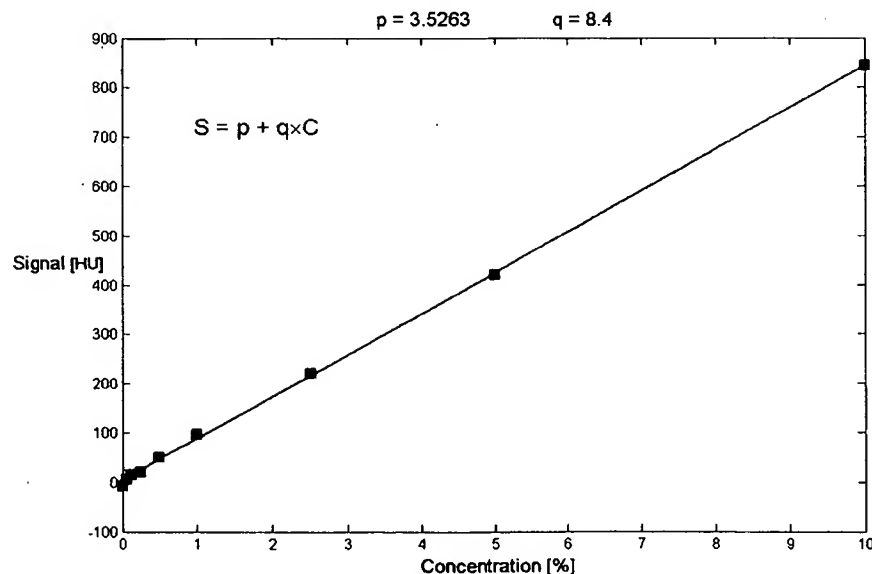
#### 1. Evaluation of the temporal variation in CT enhancement:

A series of phantom scans on a bottle containing normal saline 0.9% was performed at 3 different time points (2 weeks and 6 months apart) under the same scanning parameters used throughout the study. The signal intensity of a central axial ROI (Region Of Interest) was recorded 2-3 times in each of the 3 corresponding days. The average intensity was 39.7, 39.7 and 43.5 HU for each day, with the differences between the 2-3 readings within a specific day (up to 10 HU) being greater than the differences between the average daily readings. We conclude that the temporal variation between the signal intensities is within the noise limits of the CT scanner.

#### 2. Determining the parameters $p$ and $q$ from eq. (3):

We determined the parameters of the concentration-signal eq. (3) by preparing tubes with different concentrations of Ultravist 300 in normal saline. The tubes were scanned by the same CT protocol used in the study. Physiologically, we obtain concentrations of about 2%, which decrease with time (i.e., 1.5 ml/kg contrast agent in a 70 kg adult, results in about 100 ml contrast agent in a blood volume of about 5 lit;  $100\text{ml}/5\text{lit} = 2\%$ ). Therefore, most of the prepared concentrations,  $C$ , were within this range. In each tube we recorded the signal intensity  $S$  of a central ROI (fig. 3).

Fig. 3: The CT signal as a function of the contrast agent's concentration.



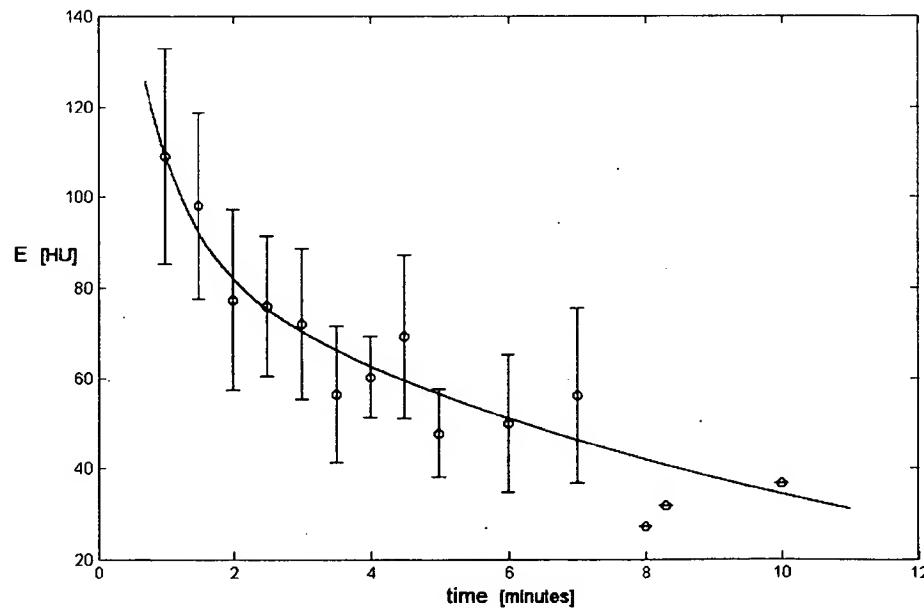
As predicted by eq. (3), the relationship is approximately linear. A minimal-square fit yields:  $p = 3.5263$  and  $q = 8.396$ . We assumed a similar slope in blood and approximated it as  $q = 8.4$ .  $p$  may be different in blood, but cancels out when we calculate the enhancement.

It has been shown previously that the CT signal enhancement was proportional to the concentration of contrast material present, and that the error associated with the calibration factor ( $q$ ) is less than 2%, rising up to 13% under theoretic refitting conditions [19,26-7].

### 3. Determining the parameters $a_1$ , $a_2$ , $m_1$ and $m_2$ :

For each patient, we choose an image slice containing the tumor. We then follow this slice along the four time points and record the signal intensity,  $S$ , of a central ROI in the aorta. We used eq. (3) to convert  $S$  to  $C_p(t)$ , as shown in **fig. 4**. Assuming similar pharmacokinetics for all patients with normal kidney function, we fit  $C_p(t)$  to eq. (1) (by the minimal-square method) to obtain:  $a_1 = 8.48$ ,  $a_2 = 7.34$ ,  $m_1 = 1.43$ ,  $m_2 = 0.1$ .

**Fig. 4:** Enhancement in the aorta as a function of time after Iopromide injection.



### b) Image analysis:

Altogether, 34 patients were enrolled in the study of whom one had two separate right lung lesions and five were found unfit to undergo image analysis due to technical acquisition problems (although two of them could contribute pharmacokinetic data). Therefore, a total of 30 lung lesions of variable diagnoses was collected. The tumor size ranged from  $2 \times 1.6 \times 0.5$  to  $7.8 \times 7 \times 12.4$  cm<sup>3</sup> with the majority under 5 cm largest diameter. Their final diagnoses (except one with macrophages per cytology waiting for another biopsy) are presented in **Table 1**:

**Table 1:** Pathological diagnoses of the lung lesions enrolled in the study.

Diagnosis*	MFH	SCLC	Ly	Breast met.	MM	NSCLC sub-type undefined	NSCLC SCC	NSCLC LCC	NSCLC Adeno-carcinoma	SFT	Benign
Number of patients	2	2	1	1	1	5	5	1	6	1	4

\*MFH – metastatic Malignant Fibrous Histiocytoma; Ly – Lymphoma;

Breast met. – Breast metastasis; MM – Multiple Myeloma; SFT – Solitary Fibrous Tumor.

Representative examples of benign and malignant tumors are shown in **figures 5-7**, consisting of thoracic CT scans of a central slice of a lesion (arrow) at  $t_1$  (**a**), color-coding of the slice (**b**), zoom of the lesion (**c**), and pathology - H&E (**d**) and cd31 (**e ± f**) staining. **Figure 8** presents the central slices of all the color-coded lesions in the study, according to final diagnoses.

While the benign lesion (**Fig. 5**) has only 34% of its pixels color-coded, the malignant one (**Fig. 6**) has 87%. Another difference is thorough coloring of the central pixels in the malignant tumor, with most of the colored pixels of the benign lesion being on its contour. Coloring of the tumor's borders is usually the result of movement of the tumor between  $t_0$  and  $t_1$ . Since the enhanced tumors are surrounded by normal lung tissue containing air (black in CT), the difference in enhancement intensity in a pixel between  $t_0$  and  $t_1$  can be large on behalf of movement of the tumor to an area of normal lung tissue (or vice versa). This occurs mainly along the contour of the tumor.

In **fig. 6** we observe a mostly red area corresponding to a region of high  $K$  and low  $v$ , neighboring a mostly blue area corresponding to a region of low  $K$  and high  $v$ . The presented pathology slices were prepared from the center of the tumor in the same plane as the CT image. Comparison yields, that red pixels represent areas of high vascularity while blue pixels represent areas of low vascularity. Furthermore, as seen on the H&E staining, the malignant tumor is vastly more cellular than the benign one, corresponding to a lower  $v$ . Accordingly, the mean brightness of the malignant lesion - 0.72, is higher than that of the benign lesion - 0.52.

**Fig. 7** represents an Adenocarcinoma. Similar to the former malignant tumor (**fig. 6**), the vast majority of the pixels within the area of the tumor are colored – 97% with a mean brightness of 0.81. Here we see a green and blue central region surrounded by a mostly red ring. This corresponds to the H&E staining showing central necrosis (high  $v$  and low  $K$ ) and to the cd31 slices showing much less vascularity in the center (**e**) than at the periphery (**f**).

**A NOVEL CT METHOD FOR LUNG CANCER DETECTION AND  
DIAGNOSIS**

**Dr. Daphna Weinstein  
Asaf Harofeh Hospital**

Supervision: Prof. Hadassa Degani  
Weizmann Institute of Science

Part C

**Fig. 5:** Cartilaginous Hamartoma (benign) with areas of fat tissue.

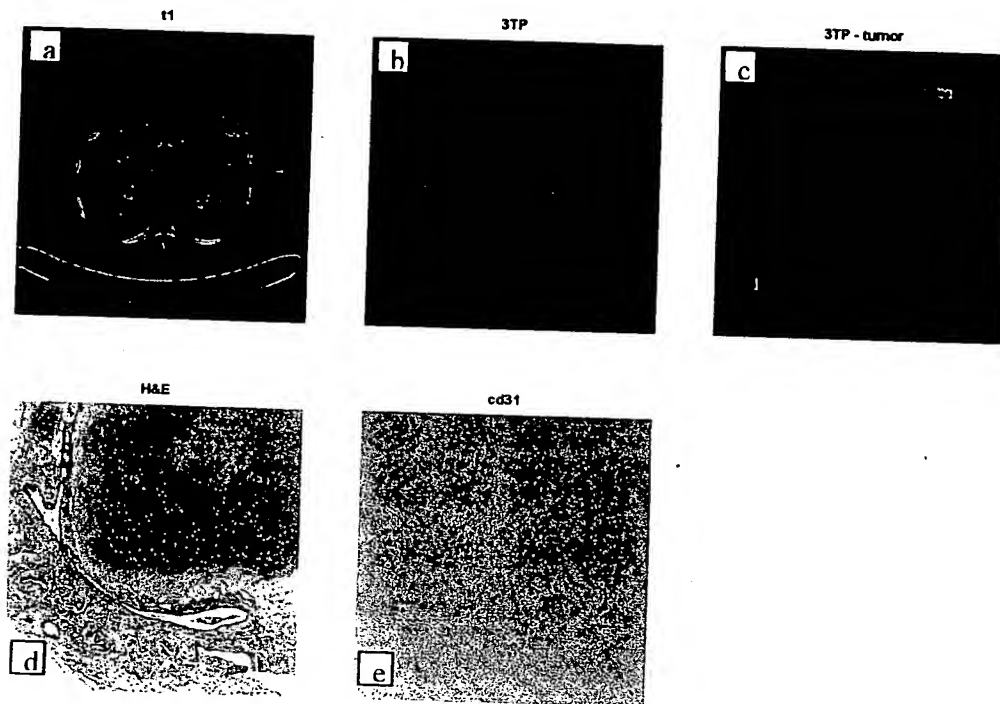
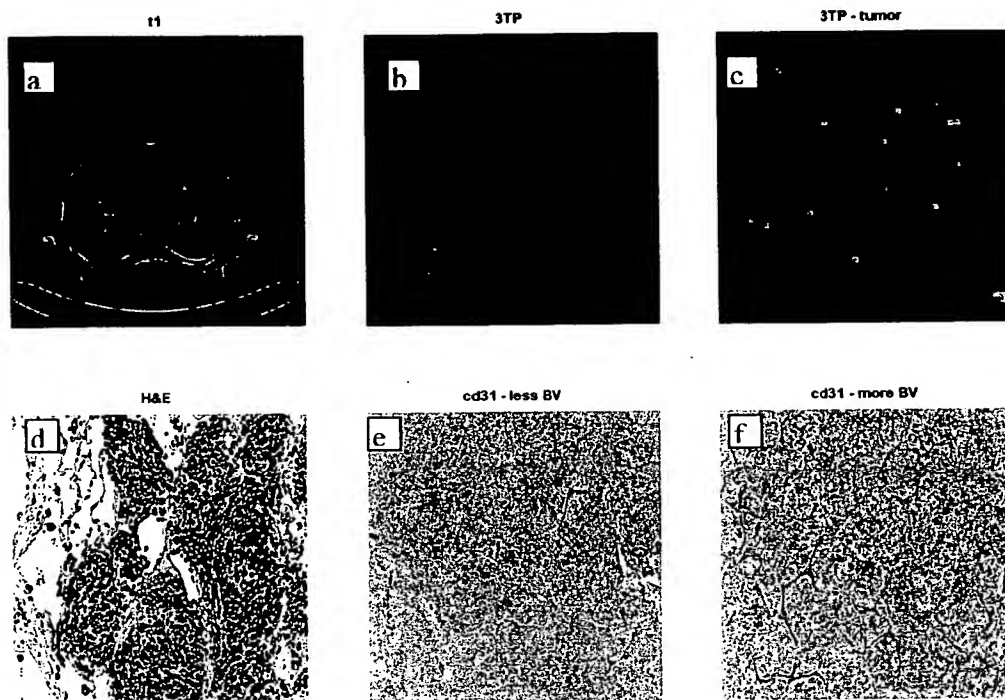
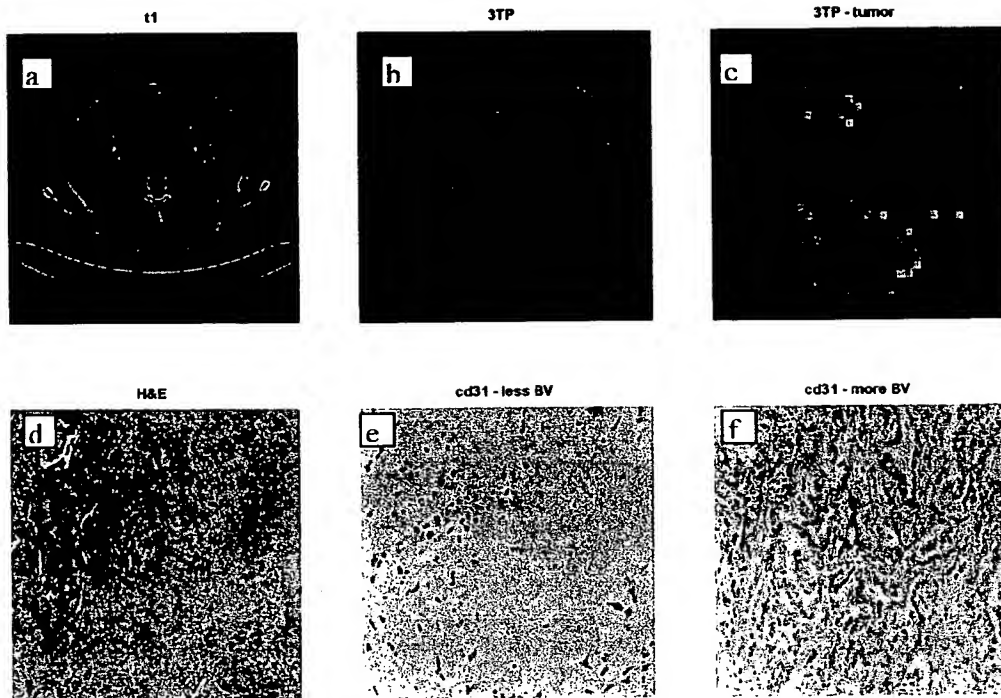


Fig. 6: Small Cell Lung Cancer.

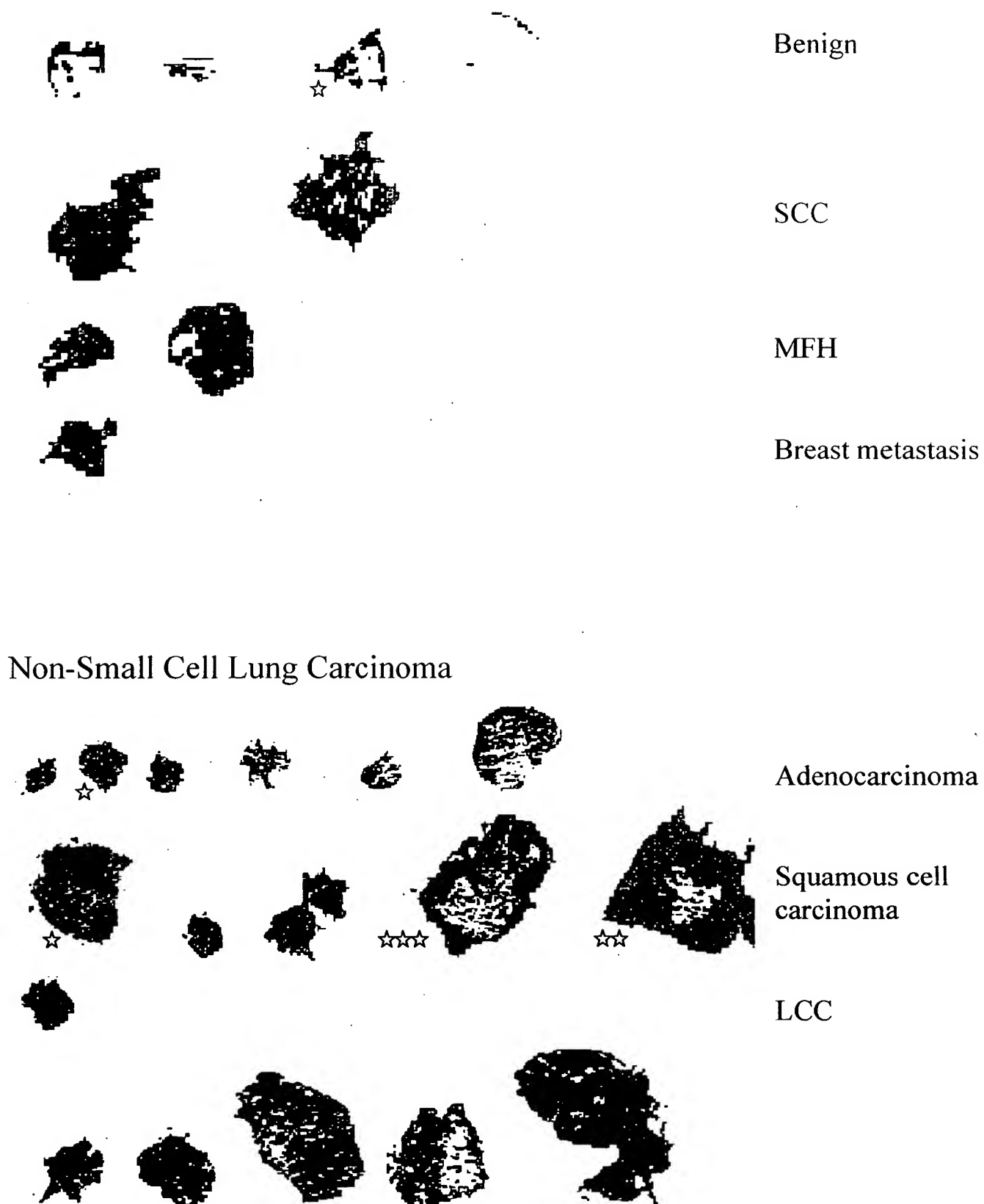


**Fig. 7: Non-Small Cell Lung Carcinoma (Adenocarcinoma).**



**Fig. 8:** Central slices of all the color-coded lesions in the study, according to final diagnoses. The presented slices represent areas between 1.4x2 and 7x9.3 cm<sup>2</sup>. As in fig. 5, in all the 4 benign cases the percent of pixels colored is low (<40%), with most of the coloring being along the borders. The benign lesion on the right turned out to be a fold of ascitic fluid surrounding the liver, for which none of the central pixels were colored. All the malignant cases are colored in 60-97% of the tumor's volume, with a median of 83%. Of course, due to the small number of benign cases included in our study, no real statistical conclusions can be reached and the above numbers serve only as possible characteristics of a benign vs. a malignant process.

Fig. 8 – central slices of all the color-coded lesions in the study, according to final diagnoses.







Multiple Myeloma

Lymphoma

Malignant Solitary  
Fibrous Tumor

In some of the large tumors, a central area of necrosis confirmed by pathology, is clearly presented by an area of sparsely colored or blue pixels (1 star). A central area of pus 3 cm in diameter is obvious as well (2 stars). The SFT (Solitary Fibrous Tumor) has necrotic foci in different dimensions. In another large tumor (3 stars) a central area of necrosis is assumed, although not confirmed pathologically since only a trucut biopsy was performed.

It is interesting to note, that both the left SCC tumor and the SFT were initially considered benign by biopsy. Since the 3TP-CT evaluation yielded a malignant appearance, further evaluation was ensued and post excision both were found to be malignant.

### **Shift:**

During image analysis it was found, that the area containing the tumor within the CT image moved between different time points, mostly due to thoracic breathing movement. The amount of movement in the z direction was evaluated by looking at sequential slices of the tumor in the 3 different time points on the screen, and forming triplets of the same slice at the 3 time points. Movement in the x-y direction was initially evaluated by putting a semi-transparent slice on top of its corresponding slice at a different time point and moving it until the best fit was found. The amount of movement in the x and y direction was recorded, and inserted into specially developed software which shifted all the pixels in the slice by the assigned amount. Later in the course of our study, an automatic shift-establishment algorithm was developed by A.W. (to be published), which was found to be superb after comparison to the manual method. Movement in the x-direction ranged between 0-20 pixels and in the y-direction between 0-12 pixels, both with a median of 2 pixels. This algorithm doesn't take into account rotation, angulation, shrinkage or enlargement of the tumor, which we ignored and presumed minimal. As a result, it is probable that the volume each pixel represents is not the exact same one along the different time points, with some of the initial pixel's volume moving into a neighboring one's. Therefore, a newer algorithm was developed, by which the color (hue and brightness) of each pixel was assigned after taking into account the values of the 8 surrounding pixels as well. This effect of "smoothing" was applied in **fig. 8**. There are 2 more reasons leading us to believe that this approach is more correct. First of all, each pixel's initial value is a result of a mathematical algorithm, which is part of the CT device. Therefore, this value includes intrinsic "noise" due to the acquisition technique and mathematical algorithm. Second of all, we are interested in histological data with a resolution capable of detecting areas of higher/lower vascularity, higher/lower cellularity, and not a higher resolution in the scale of single cells.

### **Scan times:**

As the study progressed and more pharmacokinetic data evaluated, it became clearer which  $t_1$  and  $t_2$  contribute the most valuable data. Since the contrast material's distribution is quite rapid, choosing short  $t_1$  and  $t_2$  of about 1 and 2.5 minutes enables to be near the time point of maximal enhancement. Choosing longer  $t_1$  and  $t_2$  results in a higher percent of blue pixels on the expense of red pixels, which are so characteristic of malignancy. This is made clearer by looking at the corresponding color-map (fig. 2) which shows a good representation of red and blue with a smaller area of green, which is more of a transition zone between the red and blue. Most of our data was acquired during the short time points as soon as we found they are the most suitable (of course it would have been better to compare between images all taken at the same time points).

**Fig. 9 :** SPNs - Tumors < 3cm with  $t_2 \leq 3$  min.

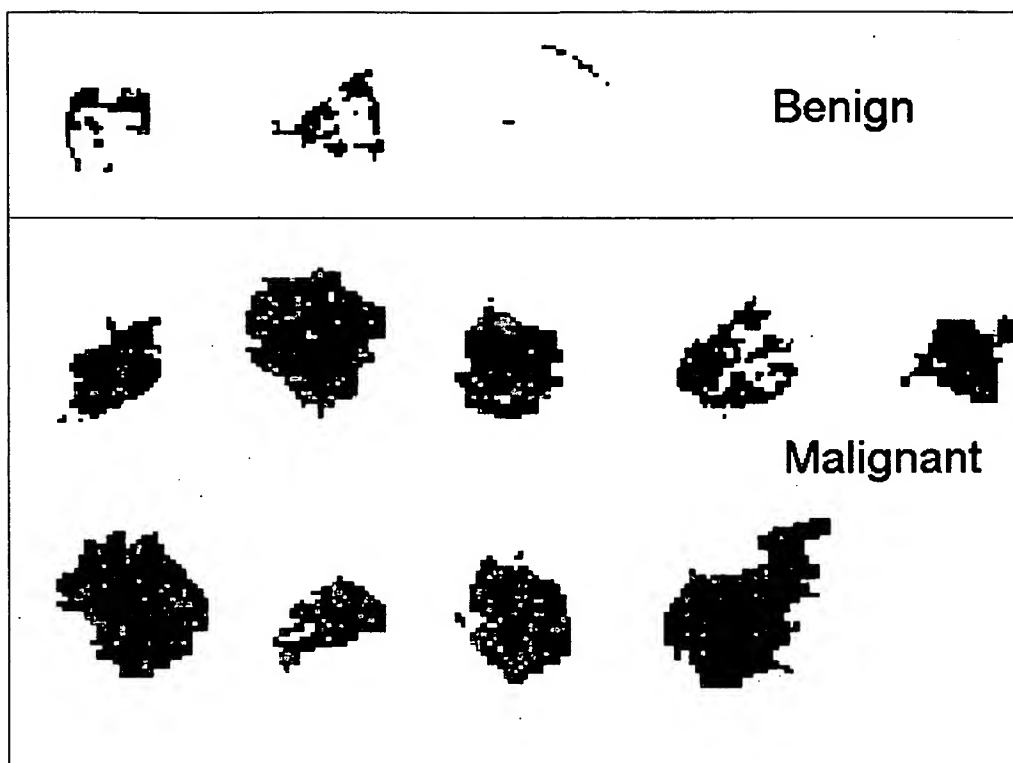


**Table 2 & 3:** statistical analysis of the images from **fig. 9**. Tab. 2 - benign, Tab. 3 - malignant.

% Vol - percent of the colored out of the total tumors' pixels

R - percent of the Red pixels out of the colored tumors' pixels

R' - percent of the red pixels out of the total pixels of the tumor

Bright - average value of color-brightness out of the colored tumors' pixels

$R_s$  - Average value of Red color-hue multiplied by the corresponding color-brightness

**Table 2:** Fig. 9's benign tumors from left to right.

Patient	%VOL	R	R'	Bright	$R_s$
1	34	58	20	0.52	61
2	38	34	13	0.39	36
3	2	100	3	0.63	100
<b>Average</b>	25	64	12	0.51	66

**Fig. 9:** Since the issue of SPNs is of utmost importance, it is interesting to look separately at a this sub-group of our tumors whose diameter is less than 3 cm. All our benign tumors fit into this category, as well as 9 of the malignant ones. Also, since we know at this point that a long  $t_2$  is not as good for our purposes a short one, we will include in this figure only images with  $t_2$  of 3 minutes or less.

**Table 3:** Fig. 9's malignant tumors from the upper left to the lower right corner.

Patient	%Vol	R	R'	Bright	R <sub>s</sub>
1	87	54	47	0.72	62
2	85	65	55	0.74	69
3	60	40	24	0.42	45
4	93	55	51	0.81	61
5	100	41	41	0.67	39
6	84	69	57	0.79	76
7	84	40	34	0.75	43
8	89	47	42	0.78	50
9	81	56	45	0.86	59
<u>Average</u>	85	52	44	0.73	56

It is quite obvious from **Fig. 9** and **tables 2 & 3** that in our sample, one can easily distinguish between a benign and malignant SPN using the 3TP-CT method (we are aware that due to the small number of benign cases the statistical data may prove invaluable). The gross differences include more coloring of the central pixels in the malignant vs. the benign tumors resulting in a higher percentage of the tumor's pixels being colored, a higher percentage of red pixels in the malignant vs. the benign tumors corresponding to richer vascularity probably due to angiogenesis characteristic of malignant neoplasms, and higher color-brightness in the malignant vs. the benign tumors due to higher cellularity.

## V) DISCUSSION

### Pharmacokinetics:

In this study we obtained:  $a_1 = 8.48$ ,  $a_2 = 7.34$ ,  $m_1 = 1.43$  and  $m_2 = 0.1$ . These values differ from the corresponding Gd-DTPA values:  $a_1 = 3.99$ ,  $a_2 = 4.78$ ,  $m_1 = 0.144$ ,  $m_2 = 0.011$  [28-9]. Possible explanations for these differences include:

1. Iopromide vs. Gd-DTPA: These contrast materials share many similarities but are not identical (i.e. both contrast agents exit the blood vessels into the extra-cellular space without entering the cells, both are eliminated almost exclusively by the kidneys and have a similar molecular weight).

2. Maximum of  $C_p(t)$ : Since our data regards short times post injection, we were able to get nearer to the maximal value of  $C_p(t)$  which occurs relatively early, and might have been missed in former pharmacokinetic studies [29-32]. If  $C_p(t)$  isn't evaluated at close times post injection, its initial steeper decline that commences after it reaches the maximum is missed. Accordingly, the values of  $a_1$ ,  $a_2$ ,  $m_1$  and  $m_2$  become lower and the half-life seems longer. This postulate is supported by the work of Krause [29], concerning the pharmacokinetics of iodinated contrast media. Regarding a similar dose and rate as in our study, maximal relative enhancement of the aorta was observed after 30 sec declining with a half-life of 11 sec and 226 sec for the bi-exponential decay.

We can approximate  $m_1 = 1$  and  $m_2 = 0.1$  for Iopromide, and  $m_1 = 0.1$ ,  $m_2 = 0.01$  for Gadolinium. Perhaps our  $m_2$  corresponds to gadolinium's  $m_1$  and our  $m_1$  corresponds to an  $m_0$  of some ultra-fast process with  $C_p(t)$  being described better by a tri-exponential equation? A potential explanation of such a rapid process could be the mixing of contrast agent in whole-body blood post injection at a specific body site, which results in "uniform" concentration throughout the whole blood volume. All our measurements were performed within 10 min from the injection where a decay time of 0.01 (gadolinium's  $m_2$ ) isn't dominant. Consequently, the distribution half-life we obtain is shorter [31].

It should be noted that our time points are measured from the beginning of injection, which actually takes about 30-40 sec, depending on the patient's weight. Therefore when  $t = 1$  min, for example, it's actually 20-30 sec post the end of the injection.

3. Dose accuracy: The actual dose might not have been exactly 1.5 ml/kg since the patients' weights were not measured precisely, but rather asked and recorded according to the patients' response. Another potential source of error, despite dosing per kg body mass, might be the empirical observation that the extracellular space is not a linear function of the mass. However, this variation is considered relatively small [29].

4. Physiology of  $a_1$  and  $a_2$ : At  $t = 0$ ,  $C_p(t) = D[a_1 + a_2]$ . Therefore  $a_1 + a_2$  must equal the total kg/lit blood in humans. Since the blood volume is 70ml/kg in males and 65 ml/kg in females [33], the mean is 67.5 ml/kg, or 14.8 kg/lit. This is relatively near our value of  $7.17 + 6.97 = 14.14$ . Also, we obtain  $C_p(t)$  from the signal intensity within a blood vessel, so it is measured in a blood volume and not in a plasma volume as done when direct measurements from blood samples is performed.

5. More possible sources of error: It has been found that interindividual variability of pharmacokinetic parameters is extremely low for iodinated contrast agents [31]. We presumed, for example, identity between males and females, between individuals of normal (but perhaps different) kidney function, that no temporal variations exist in the CT measurements, that there's ideal mixing of the contrast agent within the blood vessels in the thorax for everyone in the times measured, etc. Also, we measured the blood enhancement in the aorta at the tumor's level. So actually, the measurement wasn't performed at the exact same level within the aorta at each instance, perhaps allowing small enhancement variability. Since primary pulmonary malignancies usually derive their blood supply from the systemic (bronchial) rather than the pulmonary circulation, it was chosen to use the aorta consistently for blood enhancement measurements [27].

The signal intensities in the blood of the different patients prior to contrast injection measured 35-57.6 HU, with a median of 44.7 HU and a mean of 45.6 HU. Thus we can assume pixel noise of about  $\pm 12$  HU in the CT measurements, similar to the value of 14 found in the work of Brix *et al* [34]. Perhaps, in different CT devices different noise values will be found.

### **Image analysis:**

Angiogenesis leads to physiological changes, specifically increased perfusion, blood volume, and capillary permeability. These changes can influence contrast enhancement in CT. The ability to evaluate both the degree and distribution of tumor neovascularization is of major importance not only in diagnosing benign vs. malignant lesions, but also in predicting tumor aggressiveness. Areas of hypoxia might lead to failure of radio- and chemo-therapy, so it may prove very useful to determine such physiologic parameters by a non-invasive method such as CT. As a result, an individually tailored therapeutic approach could be planned [34].

Capillary volume represents less than 5%, and interstitial volume less than 20% in most tissues [34]. Quantitative dynamic T1-weighted contrast enhanced MRI has been used to assess tumors' mean permeability-surface area PS product and extracellular distribution space  $v$  in patients with lung cancer.

Our aim in this study was to evaluate  $K$  and  $v$  rather than to assess their exact value. The evaluation of  $K$  and  $v$  actually represents histological data, of major importance in diagnosing a

benign vs. a malignant tumor. Using the 3TP-CT method applied to pulmonary lesions, we were able to detect areas of high vs. low  $K$ , as well as areas of high vs. low  $v$ . The same capability has been studied and shown previously using the 3TP-MRI method applied to breast and prostate tumors.

One limitation of dynamic CT measurements is its radiation exposure for the patients. However, a comparable microcirculation characterization can otherwise be obtained by PET studies, which lead to a higher radiation exposure [35].

This study was performed as a pilot-study to evaluate whether the 3TP method is capable of reaching these objectives using CT imaged lung tumors. From the data collected it seems reasonable to believe it does, with especially nice results concerning SPNs. We hope in the future to collect and study more benign tumors and perhaps also more malignant ones and possibly be able to differentiate between different malignancies as well. In such a way, perhaps a novel non-invasive tool will be added to the existing ones in the effort to decrease mortality from lung cancer.



## VI) BIBLIOGRAPHY

1. Sabiston, M., *Textbook of Surgery*. 16th ed. 2001: W.B.Saunders, p.1213-28.
2. Schwartz, S.S., *Principles of Surgery*. 6th ed. Vol. 1. 1994: McGraw-Hill, Inc, p.737-53.
3. Montesano, R., and Hall, J. *Environmental causes of human cancers*. *Europ. J. Cancer*, 2001, 37: S67-S87.
4. Ellis, J.R. and Gleeson F.V. *Lung cancer screening*. *Br J Radiol*, 2001, 74:478-85.
5. Patz, E.F., Jr. *Imaging bronchogenic carcinoma*. *Chest*, 2000, 117(4 Suppl 1):90S-95S.
6. The World Health Organization histological typing of lung tumors. Second edition. *Am J Clin Pathol*, 1982, 77(2):123-36.
7. Goldberg, M., and Unger M., *Lung cancer. Diagnostic tools*. *Chest Surg Clin N Am*, 2000, 10:763-79.
8. Diederich, S., et al. *Screening for asymptomatic early bronchogenic carcinoma with low dose CT of the chest*. *Cancer*, 2000. 89(11 Suppl):2483-4.
9. Kauczor, H.U., and Kreitner, K.F. *Contrast-enhanced MRI of the lung*. *Eur J Radiol*, 2000, 34:196-207.
10. Haberkorn, U., and Schoenberg, S.O., *Imaging of lung cancer with CT, MRT and PET*, *Lung Cancer* 2001, 34:s13-s23.
11. Boiselle, P.M., Ernst, A., and Karp, D.D. *Lung cancer detection in the 21st century: potential contributions and challenges of emerging technologies*. *AJR Am J Roentgenol*, 2000, 175:1215-21.
12. Lam, S., and Shibuya, H. *Early diagnosis of lung cancer*. *Clin Chest Med*, 1999, 20:53-61.
13. Lam, S., et al. *Localization of bronchial intraepithelial neoplastic lesions by fluorescence bronchoscopy*. *Chest*, 1998, 113:696-702.
14. Swensen, S.J., et al., *Lung nodule enhancement at CT: multicenter study*. *Radiology*, 2000, 214: 73-80.
15. Shaham, D. and Guralnik, L. *The solitary pulmonary nodule: radiologic considerations*. *Semin Ultrasound CT MR*, 2000. 21(2): 97-115.
16. Reeves, A.P. and Kostis, W.J. *Computer-aided diagnosis of small pulmonary nodules*. *Semin Ultrasound CT MR*, 2000. 21(2): 116-28.
17. Aberle, D.R., et al. *A consensus statement of the Society of Thoracic Radiology: screening for lung cancer with helical computed tomography*. *J Thorac Imaging*, 2001, 16:65-8.
18. Schering. *Ultravist - Annotated corporate core text/CDLS*, 2000: 1-28.
19. Lee, T.Y., Ellis, R.J., Dunscombe, P.B., McClarty, B., Hodson, D.I., Kroeker, M.A., and Bews, J. *Quantitative computed tomography of the brain with Xenon enhancement: a phantom study with the GE9800 scanner*. *Phys Med Biol.*, 1990, 35(7):925-935.

20. Kelcz, F., Furman-Haran, E., Grobgeld D., and Degani, H. *Clinical Testing of High-Spatial-Resolution Parametric Contrast-Enhanced MR Imaging of the Breast*. AJR, in press 2002.
21. Degani, H., Gusis, V., Weinstein, D., Fields S., and Strano S. *Mapping pathophysiological features of breast tumors by MRI at high spatial resolution*, Nature Medicine, 1997, 3:780-782.
22. Weinstein, D., Strano, S., Cohen, P., et al S. *Mapping Pathophysiologic Features of Breast Fibroadenoma by the Three Time Point (3TP) Contrast Enhanced MRI Method; Pilot Study*, Radiology, 1999, 210:233-40.
23. Furman-Haran, E., and Degani, H. *Parametric analysis of breast MRI*. J Comput Assist Tomogr. , 2002, 26:376-86.
24. Tofts, P.S., and Kermode, A.G. *Measurement of the blood-brain barrier permeability and leakage space using dynamic MR imaging. 1. Fundamental concepts*. Magn Reson Med, 1991, 17:357-67.
25. Kety, S.S. *The theory and application of the exchange of inert gas at the lungs and tissues*. Pharmacol. Rev., 1951, 3:1-41.
26. Yeung, W.T., Lee, T.Y., Del Maestro, R.F., Kozak, R. and Brown, T. *In vivo CT measurement of blood-brain transfer constant of iopamidol in human brain tumors*. J. Neurooncol., 1992, 14:177-187.
27. Miles, K.A., Griffiths M.R., and Fuentes, M.A. *Standardized perfusion value: universal CT contrast enhancement scale that correlates with FDG PET in lung nodules*. Radiology, 2001, 220:548-553.
28. Tofts, P.S., and Berkowitz B.A. *Measurement of capillary permeability from the Gd enhancement curve: A comparison of bolus and constant infusion injection methods*. Magn Reson Imaging, 1994, 12:81-91.
29. Krause, W. *Application of Pharmacokinetics to computed Tomography. Injection rates and Schemes: Mono-, Bi-, or Multiphasic?* Invest Radiol, 1996, 31(2):91-100.
30. Weinmann, H.J., Lajniado, M., and Mutzel, W. *Pharmacokinetics of Gd-DTPA /Dimeglumine after bolus injection into healthy volunteers*. Phys Chem Phys Med NMR, 1984, 16:167-172.
31. Krause, W., Schuhmann-Giampieri, G., Staks, T., and Kaufman J. *Dose proportionality of iopromide pharmacokinetics and tolerability after IV injection in healthy volunteers*. Eur J Clin Pharmacol., 1994, 46:339-343.
32. Hartwig, P., Mutzel, W., and Taenzer, V. *Pharmacokinetics of iohexol, iopamidol, iopromide, and iosimide compared with meglumine diatrizoate*. Fortschr Geb Rontgenstrahlen Nuklearmed Ergänzungsbd, 1989, 128:220-3.
33. Marino, P.L., *The ICU book*, 2nd ed. 1997, William & Wilkins, p.873.

34. Brix, G., Bahner, M.L., Hoffman, U., Horvath A., and Schreiber W. *Regional blood flow, capillary permeability, and compartment volumes: measurement with dynamic CT - initial experience*. Radiology, 1999, 210:269-276.
35. Hunter, G.J., Hamberg, L.M., Choi, N., Jain, R.K., McCloud, T., and Fischman, A.J. *Dynamic T1-weighted magnetic resonance imaging and positron emission tomography in patients with lung cancer: correlating vascular physiology with glucose metabolism*. Clin cancer res, 1998, 4(4):949-55.